VISSR ATMOSPHERIC SOUNDER

Monthly Progress Report No. 8
For the Period 1 April 1974 to 30 April 1974

Contract No. NAS5-21965

For National Aeronautics and Space Administration
Goddard Space Flight Center
Glen Dale Road
Greenbelt, Maryland 20771

By

V. E. Suomi, Principal Investigator
L. A. Sromovsky, Co-Investigator

The University of Wisconsin
Space Science and Engineering Center
1225 West Dayton Street
Madison, Wisconsin 53706

INTRODUCTION

This month begins a series of reports describing the improvements and new results of the VAS computer simulation program. Although results are still meager at this time, the basic elements of the simulator have been implemented and debugged. The attached report, prepared by Dr. H. Revercomb, describes the theory and procedures used to calculate realistic spatial weighting functions for the VAS instrument. Other aspects of the simulator will be dealt with in subsequent reports.

SPATIAL WEIGHTING FUNCTIONS

Introduction:

The spatial weighting functions for use in simulations were extended to better represent the effect of diffraction. The new functions are finite over a square 8 mr on a side approximately centered at the detector IGFOV. This square FOV contributes about 99.75% of the total detector response for the 11.2μ channel. Mathematically the spatial weighting functions, $\phi(x,y)$, are defined as follows:

$$I(t) = \int_{-\infty}^{\infty} dx \int_{-\infty}^{\infty} dy \; \phi(x-x_o(t),\, y-y_o(t))\; I_s(x,y)$$

where $I_s(x,y)$ is the scene radiance as a function of position (x,y) and $I(t)$ is the measured radiance at time t when the detector IGFOV is centered a (x_o, y_o). The normalization condition on ϕ is:

$$\int_{-\infty}^{\infty} dx \int_{-\infty}^{\infty} dy\ \phi(x,y) = 1$$

such that $I_s(x,y)$ is the scene radiance when the scene is uniform. The spatial weighting function can be written in terms of the diffraction function D and the detector output filter impulse response function R as follows:

$$\phi(x-x_o,y) = N \int_{-\infty}^{\infty} dx'\ R\ (\frac{x_o-x'}{v})\ D(x-x',y)$$

N is the normalization constant. $R\ (\frac{x-x'}{v})$ is the fraction of the detector output at time x/v due to the detector output at time x'/v (v is the speed of the IGFOV center). D (x-x',y) is the fractional energy entering the optical system from scene position (x,y) which falls on the detector while its IGFOV is centered at (x',y). (It should be noted that the detector responsivity was assumed to be uniform in the above definition of ϕ).

In this report we discuss the diffraction function and the approximation to it used for simulation, and then illustrate the results of numerical calculations of the diffraction functions and the spatial weighting functions for bands 1, 5, 7, 8, 10 and 12.

1.0 Asymptotic Behavior of the Diffraction Function and Detector Sensitivity to Radiation from Outside its IGFOV.

The diffraction function D(x,y) which represents the fraction of the energy incident on the optical system from position (x,y) of the scene that is diffracted onto the detector can be written specifically as:

$$D(x,y) = \frac{\int_{A_d} d\xi' d\eta' I_d([\xi(x)-\xi']^2 + [\eta(y)-\eta']^2)}{\int_o^{\infty} I_d(r)\, 2\pi R dR} \qquad (1)$$

where the integral is taken over the detector area A_d; $\xi(x)$ and $\eta(y)$ are the projections on the focal plane of the scene position (x,y); and $I_d(R)$ is the diffracted intensity on the focal plane at a distance R from the geometrical projection of a point source in the scene. The diffracted intensity is that of an annular aperture and is given by (Born, 1965)

$$I_d(r) = \frac{I_o}{(1-\varepsilon^2)^2} \left[\frac{2J_1(\rho)}{\rho} - \varepsilon^2 \frac{2J_1(\varepsilon\rho)}{\varepsilon\rho}\right]^2 \qquad (2)$$

where $\rho = 2\pi \frac{a}{\lambda} \sin r$; r is the angular position of the point source.

a = outer aperture radius

λ = wavelength of diffracted radiation

ε = obscuration ratio (inner aperture radius = a)

J_1 = first order Bessel function

I_o = the intensity at r = 0

From D(x,y) we can determine the fractional energy incident on the detector from within a circle of angular radius r defined by:

$$E(r) = \frac{\iint_{circle} D(x,y)dxdy}{\int_{-\infty}^{\infty} dx \int_{-\infty}^{\infty} dy D(x,y)}$$

$$= \frac{1}{A_d} \iint_{circle} D(x,y)dxdy. \qquad (3)$$

E(r) is a measure of the detector response (for uniform detector responsivity) to radiation from outside of its IGFOV.

1.1 Asymptotic Behavior of D(x,y)

For source points very distant from the center of the detector IGFOV, the diffraction function becomes radial and can be approximated analytically

by using the asymptotic expansion of the Bessel functions of Equation 2. This approximation is useful for determining E(r) for large r.

First consider the point diffraction pattern expressed by Equation 2. For our application the argument of the Bessel functions is large for r larger than the IGFOV of the detector. Using the following representative parameter values:

side of square IGFOV: .384 mr

λ : 11.17 μ

a : 20.3 cm

r : .2 mr,

we see that

$$\rho = 2\pi\frac{a}{\lambda} \sin r \doteq \frac{2\pi a}{\lambda} r = 22.8.$$

Therefore, the Bessel function can be approximated to within a few percent by:

$$J_1(\rho) \doteq \left(\frac{2}{\pi\rho}\right)^{1/2} \cos\left(\rho - \frac{3\pi}{4}\right) \tag{4}$$

We can see that the oscillations of the point diffraction function as r is varied are very rapid. If the obscuration ratio were 0 (it is actually .4) minima of the diffraction pattern would occur at intervals of $\frac{\lambda}{2a}$ = .028 mr for λ = 11.17μ. About 14 minima occur over the area of the detector. Substituting the approximation of Equation 4 into Equation 2 gives:

$$I_d(r) \doteq \frac{I_o}{(1-\varepsilon^2)^2} \frac{8}{\pi} \frac{1}{\rho^3} \left[\cos^2\left(\rho - \frac{3\pi}{4}\right) + \varepsilon\cos^2\left(\varepsilon\rho - \frac{3\pi}{4}\right) - 2\sqrt{\varepsilon}\cos\left(\rho - \frac{3\pi}{4}\right)\cos\left(\varepsilon\rho - \frac{3\pi}{4}\right)\right]$$

Since for large 4, the variable ρ does not change very much over the detector area and because the cosine functions go through many oscillations over the detector, the integral of $I_d(r)$ over A_d can be approximated by:

$$\int_{A_d} I_d(r)\,da \doteq \frac{I_o}{(1-\varepsilon^2)^2}\, A_d\, \frac{1}{\pi^4}\, \left(\frac{\lambda}{a}\right)^3 \left(\frac{1+\varepsilon}{2}\right) \frac{1}{r^3} \tag{5}$$

where r is the angular distance of the point source from the center of the IGFOV. The factor ρ^{-3} was removed from the integral and the cosine integrals were replaced by their average over integer numbers of cycles. The fractional error caused by removing ρ^{-3} from the integral can be approximated by $\frac{d^2}{2r^2}$ where d is the side of the detector square. The exact integral oscillates about the approximation of Equation 5 because of the cosine integral approximation, however, the amplitude is small and the frequency large so that the average over a small change in r is well represented by the approximation.

We have essentially obtained the asymptotic diffraction function including its wavelength dependence. Noting that the integral of the point diffraction pattern over all angles r is proportional to λ^2 (using $\sin r \doteq r$) we have from Equation 5:

$$D(r) \approx A_d \frac{K\lambda}{r^3}$$

where K is a proportionality constant which is wavelength independent.

1.2 Asymptotic Behavior of E(r) and Energy Circles

Using the asymptotic diffraction function we can easily determine the fractional energy incident on the detector from outside a circle with large angular radius r. That is, we can find 1-E(r):

$$\begin{aligned} L\text{-}E(r) &= \frac{1}{A_d} \int_r^\infty D(r')\,2\pi r'\,dr' \\ &= 2\pi K \frac{\lambda}{r} \end{aligned}$$

TABLE 1.1. WAVELENGTH DEPENDENCE OF DETECTOR EFFECTIVE IFOV

	Fraction of total response originating from within a circle of indicated radius (mr)				
WAVELENGTH	50%	80%	90%	99%	99.9%
3.73	.138	.175	.187	.310	3.10
6.71	.140	.179	.195	.561	5.61
11.17	.143	.187	.219	.928	9.28
14.71	.146	.195	.240	1.222	12.22
11.17a	.076	.107	.148	.928	9.28

a .192 mr detector. All other wavelengths are for a .384 mr detector.

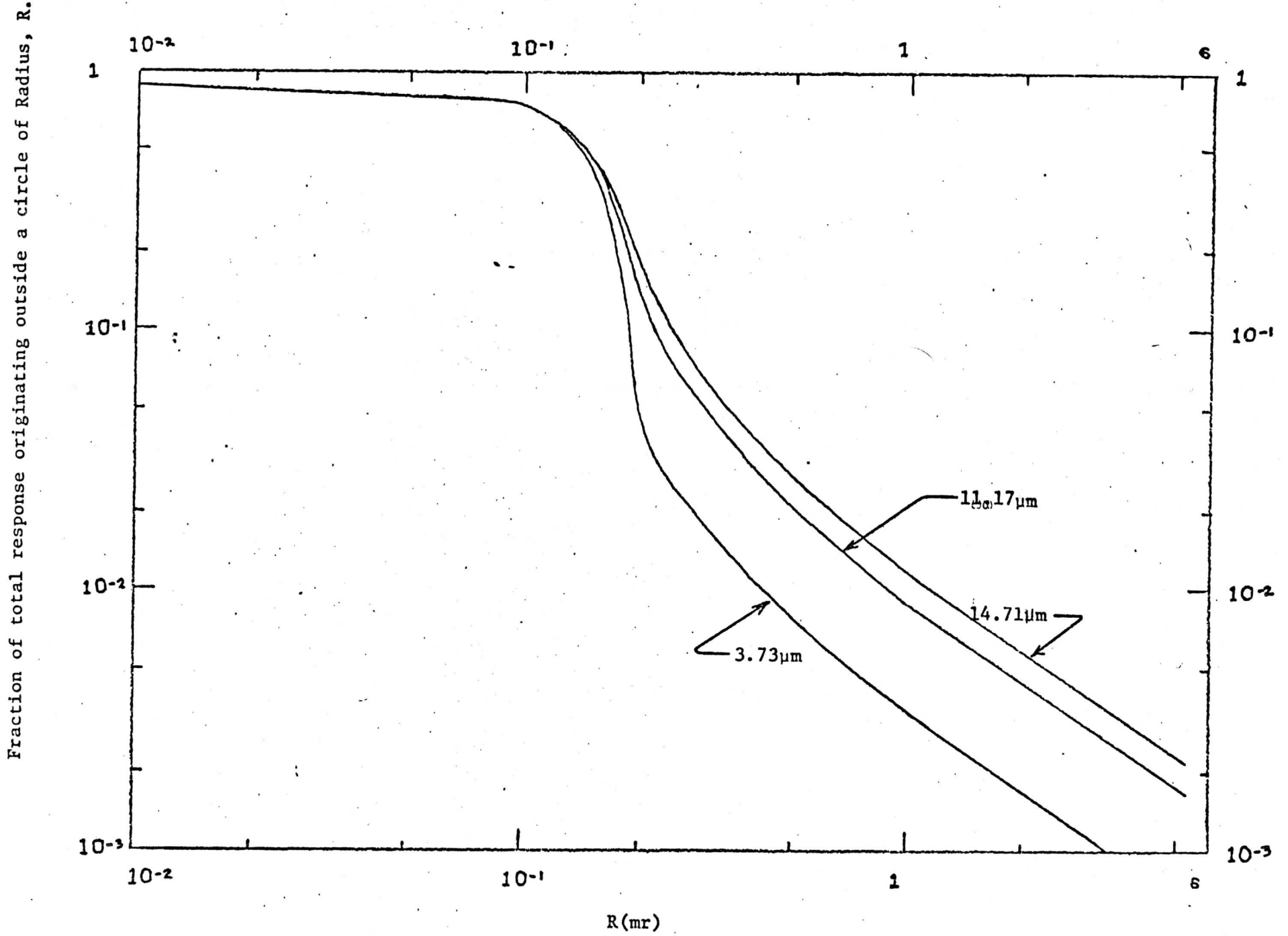

FIGURE 1.1. DIFFRACTION VARIATIONS WITH WAVELENGTH

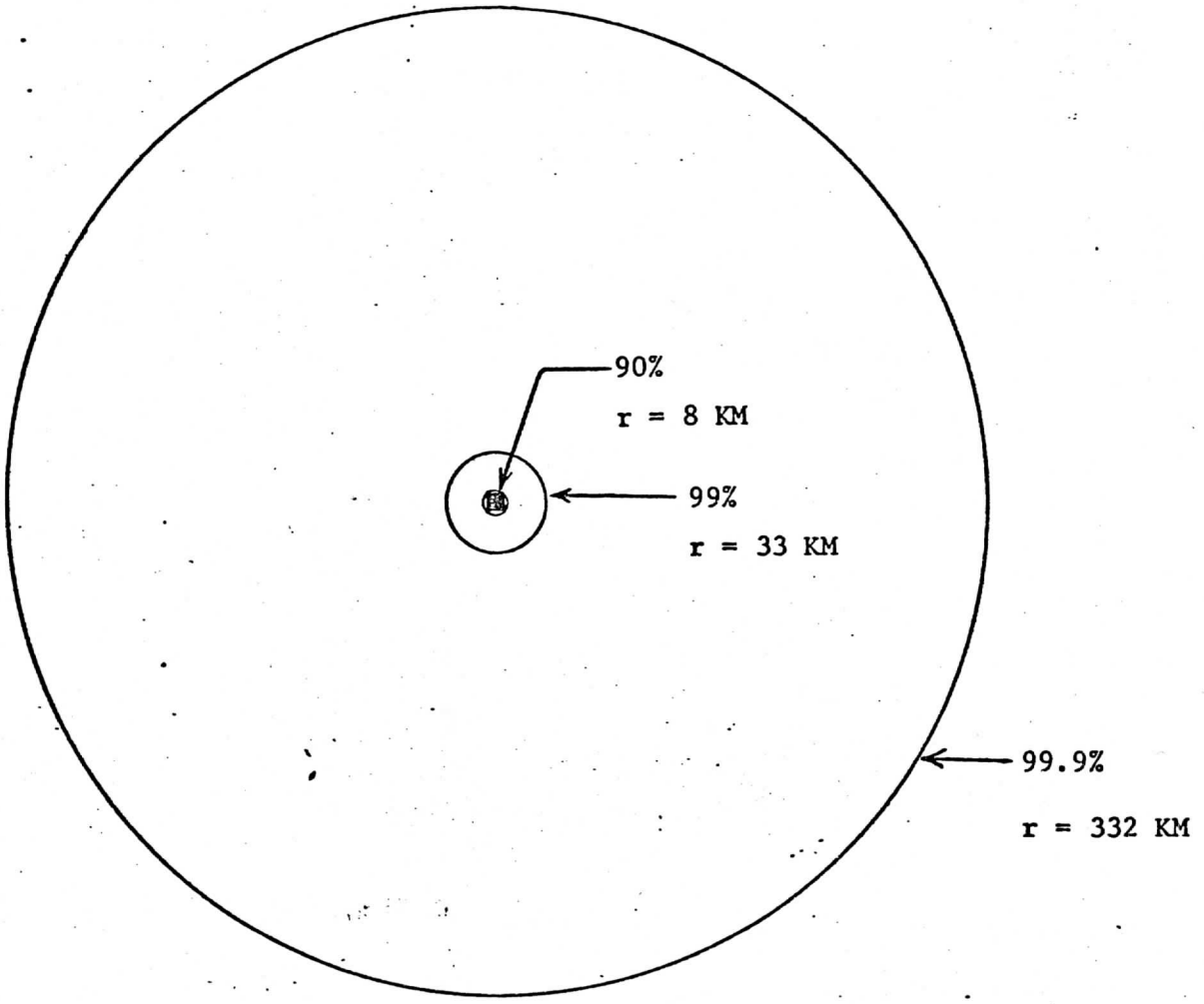

FIGURE 1.2. 11.2μ Energy Circles. The % values indicate the amount of detector response originating from inside of a circle of radius r given in terms of subsatellite distances. The dark square is the detector IGFOV.

Then for r larger than about 1 mr the angular radius of a circle containing the fraction E(r) of the total detector response is:

$$r = 2\,K\,\frac{\lambda}{1-E(r)} \quad . \tag{7}$$

For r smaller than 1 mr the diffractive response was calculated numerically using Equations 6 and 7 to extend the necessary integrals to r large. Also the predictions of Equations 6 and 7 were verified and the constant K was found to have the value 1.32×10^{-4} when x is measured in microns, r in milliradians, and A_d in $(mr)^2$. The results are shown in Figure 1.1 and some values are given in Table 1.1. The numerical results are approximate because the diffraction function was assumed to be radial. D(r) was approximated by D(x,y) with y = 0. The results are shown more dramatically in the form of energy circles on the earth about the subsatellite point in Figure 1.2.

2.0 Two-Dimensional Diffraction Function for use in Simulations

The diffraction function D(x,y) for a square detector is a two-dimensional function. In spite of its obvious symmetries (if the detector responsivity is assumed uniform) numerical calculation of the total function would require a large amount of computer time. As an alternative, we have for simulation purposes calculated D(x,y = 0) and used it, in conjunction with the results in Section 1.0, to form an approximation to D(x,y).

We noted in Section 1.0 that as x or y become large the diffraction function becomes radial, i.e. $D(x,y) \rightarrow D(x^2 + y^2)$. To incorporate this behavior into the approximate D(x,y) we use different functional forms over the two regions shown in Figure 1.3. In the shaded "star" region

the square symmetries of the detector are expressed by letting:

$$D(x,y) = D(x,0)\ D(0,y) \tag{8}$$

For points outside of the "start", a radial function is constructed which is continuous with the inside function at the boundaries. As defined in Figure 1.3 the points (x_0,y_0) and (y_0,x_0) lie on the intersection of a circle centered at the center of the detector IGFOV and passing through (x,y). For the general case where the detector responsivity is not uniform a diffraction function of the following form is assumed:

$$D(x,y) = \sin^2\Theta\ D(x_0,y_0) + \cos^2\Theta\ D(y_0,x_0) \tag{9}$$

where Θ is defined in the figure and

$$D(x_0,y_0) = D(x_0,0)\ D\ (0,y_0).$$

If the responsivity is uniform this reduces to the radial function,

$$D(x,y) = D(x_0,0)\ D\ (0,y_0). \tag{10}$$

The side of the square d inside of which the diffraction function is given by Equation 8 was chosen to be .44 mr for the large detector (.4 mr square) and .22 mr for the small detector (.2 mr square). As mentioned earlier the diffraction functions were calculated for an 8 x 8 mr square which includes 99.75% of the detector response for a wavelength of 11.17μ.

3. Numerical Results for the Diffraction Functions and the Spatial Weighting Functions

The diffraction functions for channels 1,5,7,8,10,12 are shown in Figure 1.4. The semilog plots, which greatly accentuate the large angle tails, represent a cross-section of D parallel to the sides of the IGFOV and passing through its center, (i.e. D(x,o)). The oscillations of the tails of the functions for the long wavelength plots are caused by oscillations of the diffraction pattern for a point source. The large angle behavior of the diffraction functions is consistent with the

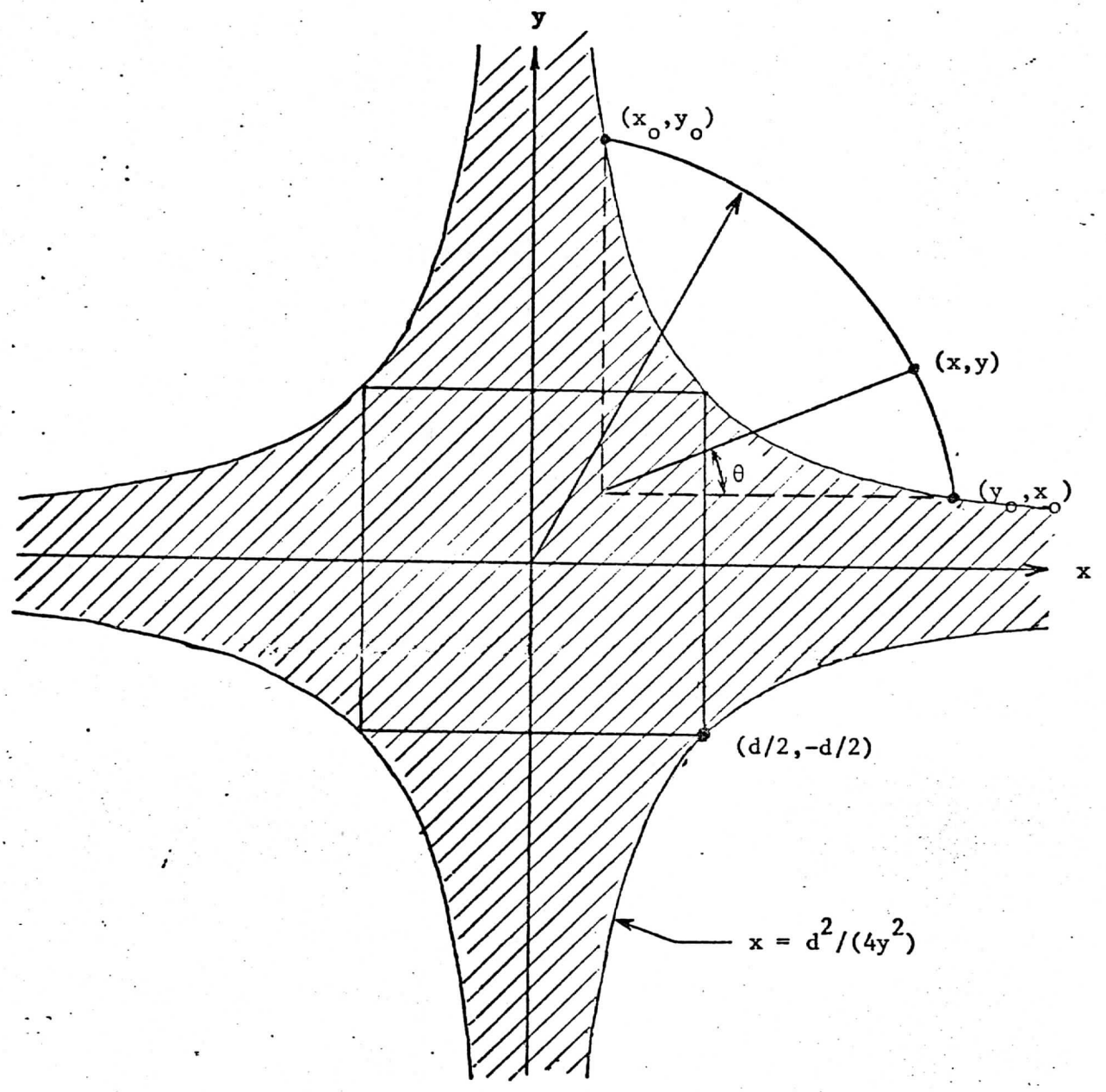

Figure 1.3. Illustration of the procedure for generation of two-dimensional diffraction functions

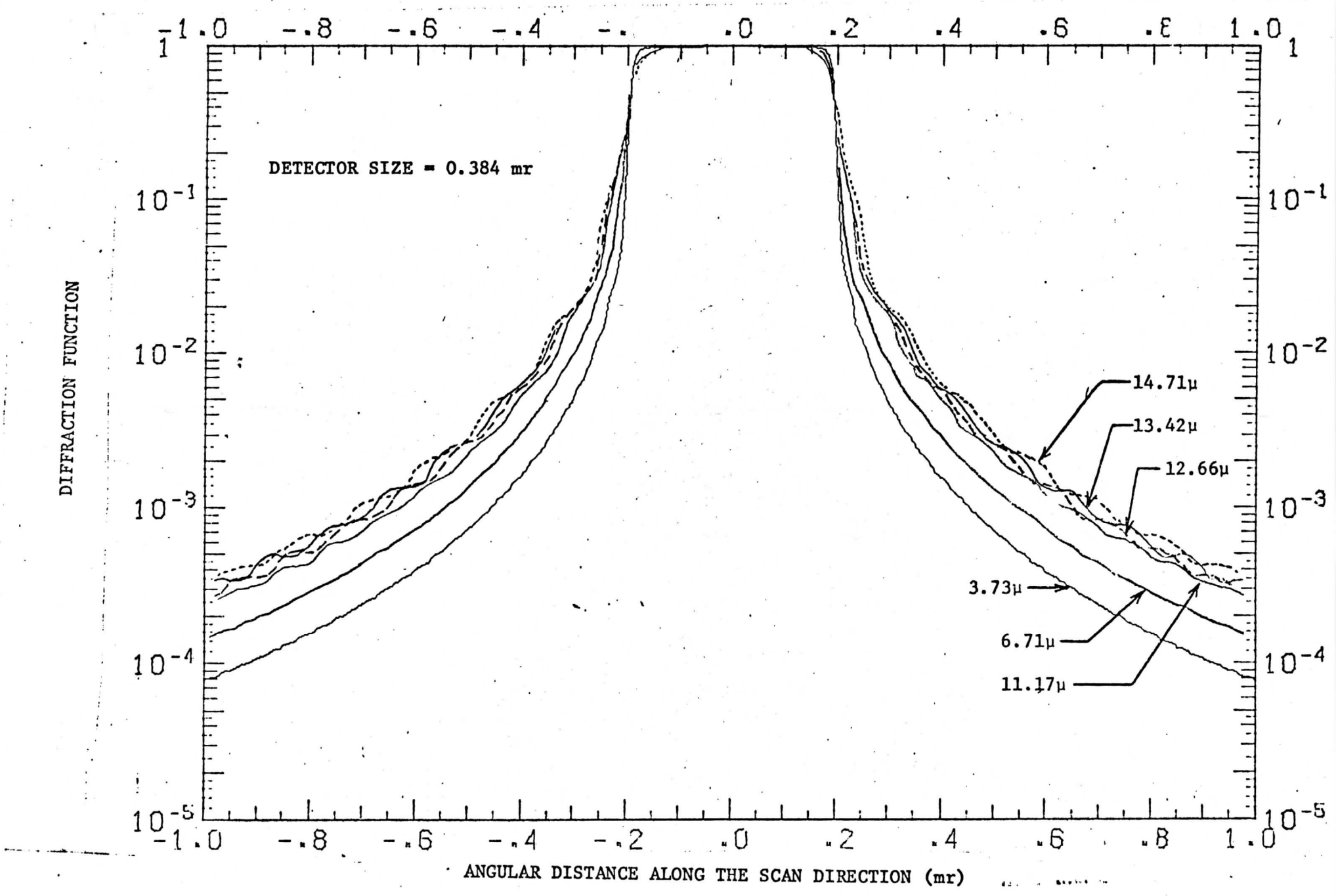

FIGURE 1.4. Diffraction functions for bands 1,5,7,8,10 and 12 are all shown for a detector size of 0.384 mr

discussion of Section 1.0.

The spatial weighting functions for channels 1,5,7,8,10 are shown in Figure 1.5 and 1.6. The plots represent east-west slices of ϕ; since we are assuming a uniform detector responsivity the north-south slices are identical to the diffraction functions. The oscillations noticeable in the semilog plots are caused by oscillations of the impulse response function and are largest for channels where the diffraction function falls off the sharpest. For very large angles, ϕ and D become essentially identical because the impulse response function is a sharply peaked function.

The band 12 spatial weighting function is shown in Figure 1.7 and 1.8. To illustrate the difficulty of registering band 12 with the HgCdTe window band, band 8 weighting functions are also included. A 100% linear modulation of the detector responsivity was included in the band 8 spatial weighting functions, while the responsivity was assumed uniform for band 12.

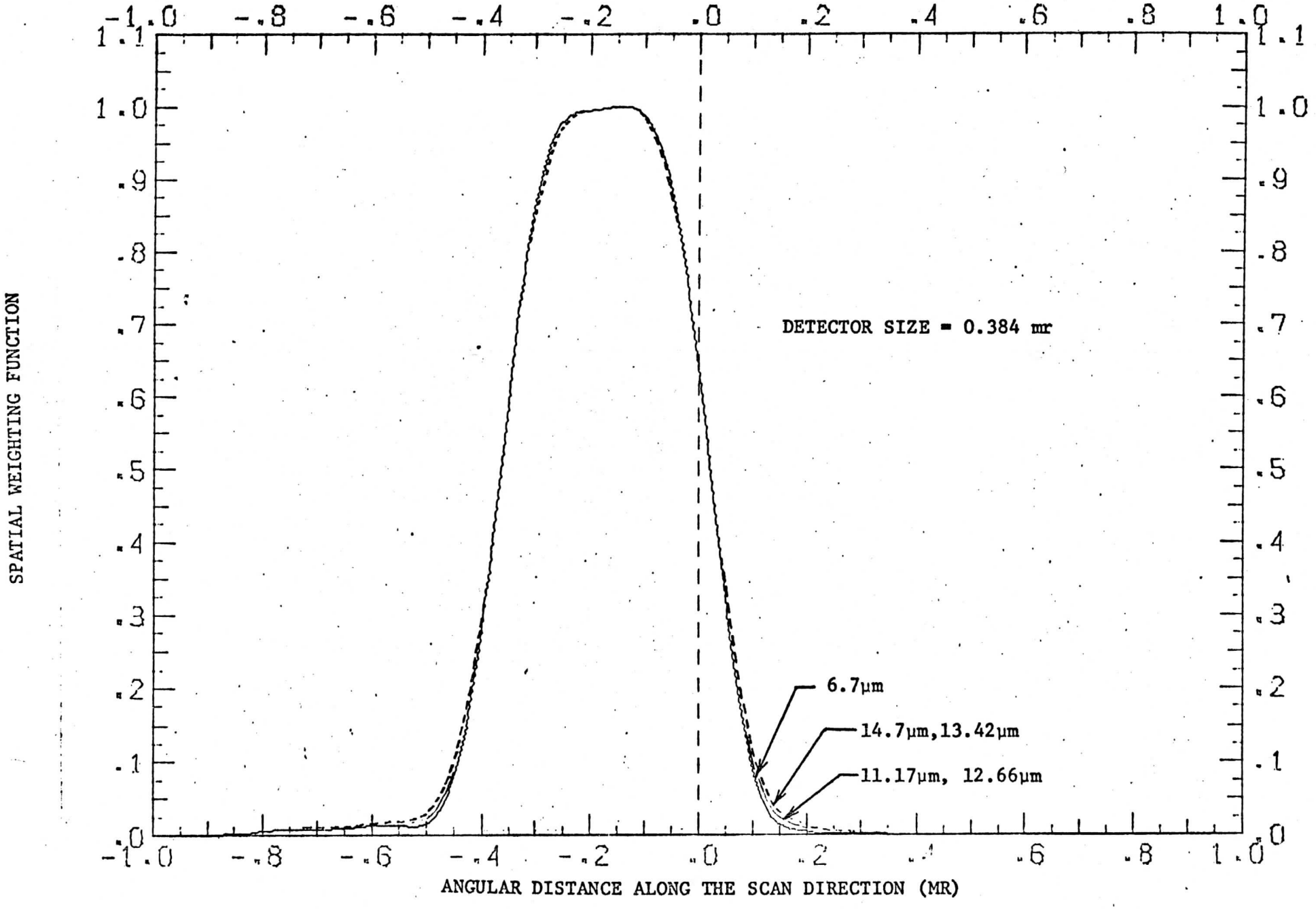

Figure 1.5. Spatial weighting functions for bands 1,5,7,8, and 10. Non-uniform responsivity of

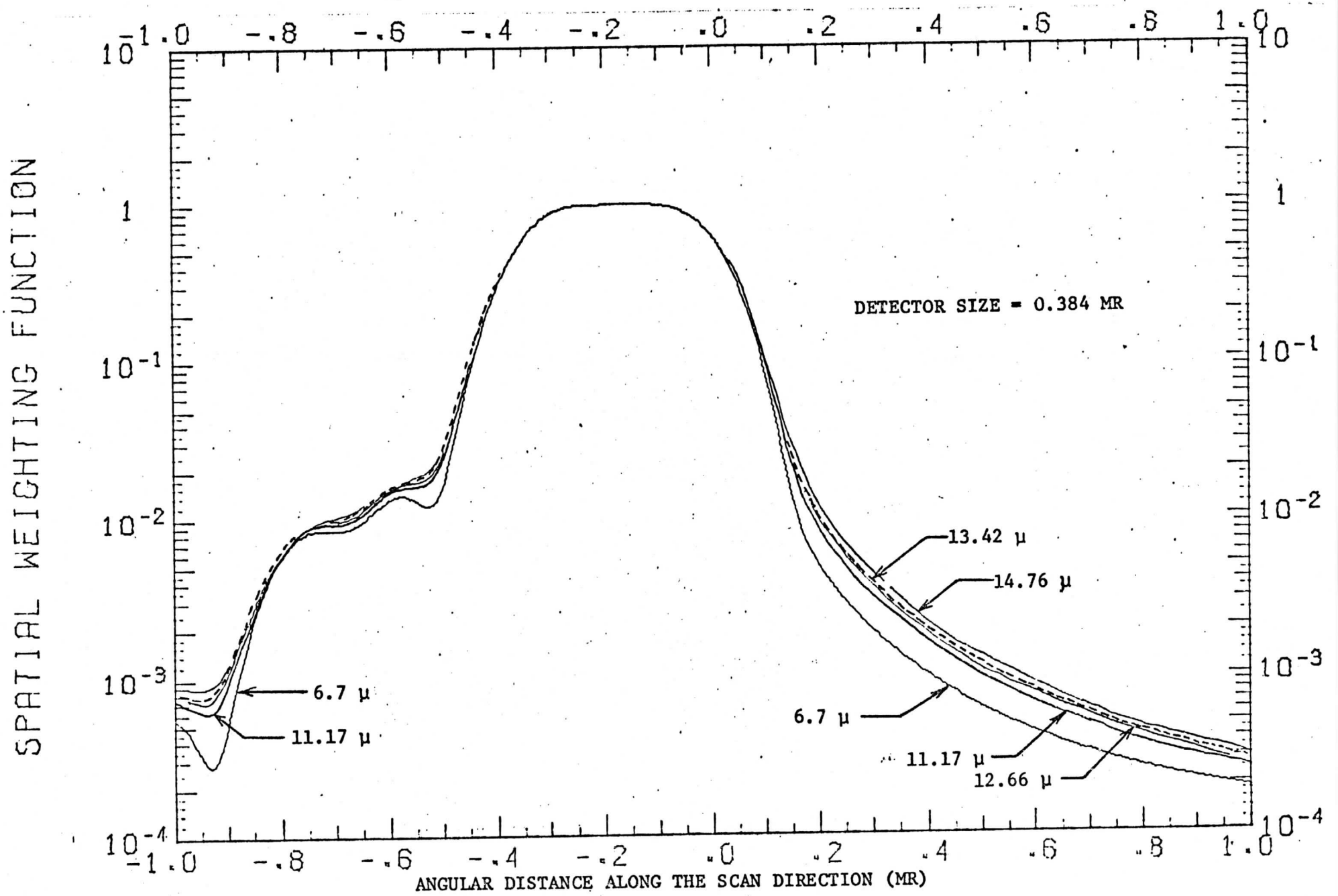

Figure 1.6. Semi-log version of Figure 3.2. Except for the 6.7μ case all bands plotted show extremely small differernces.

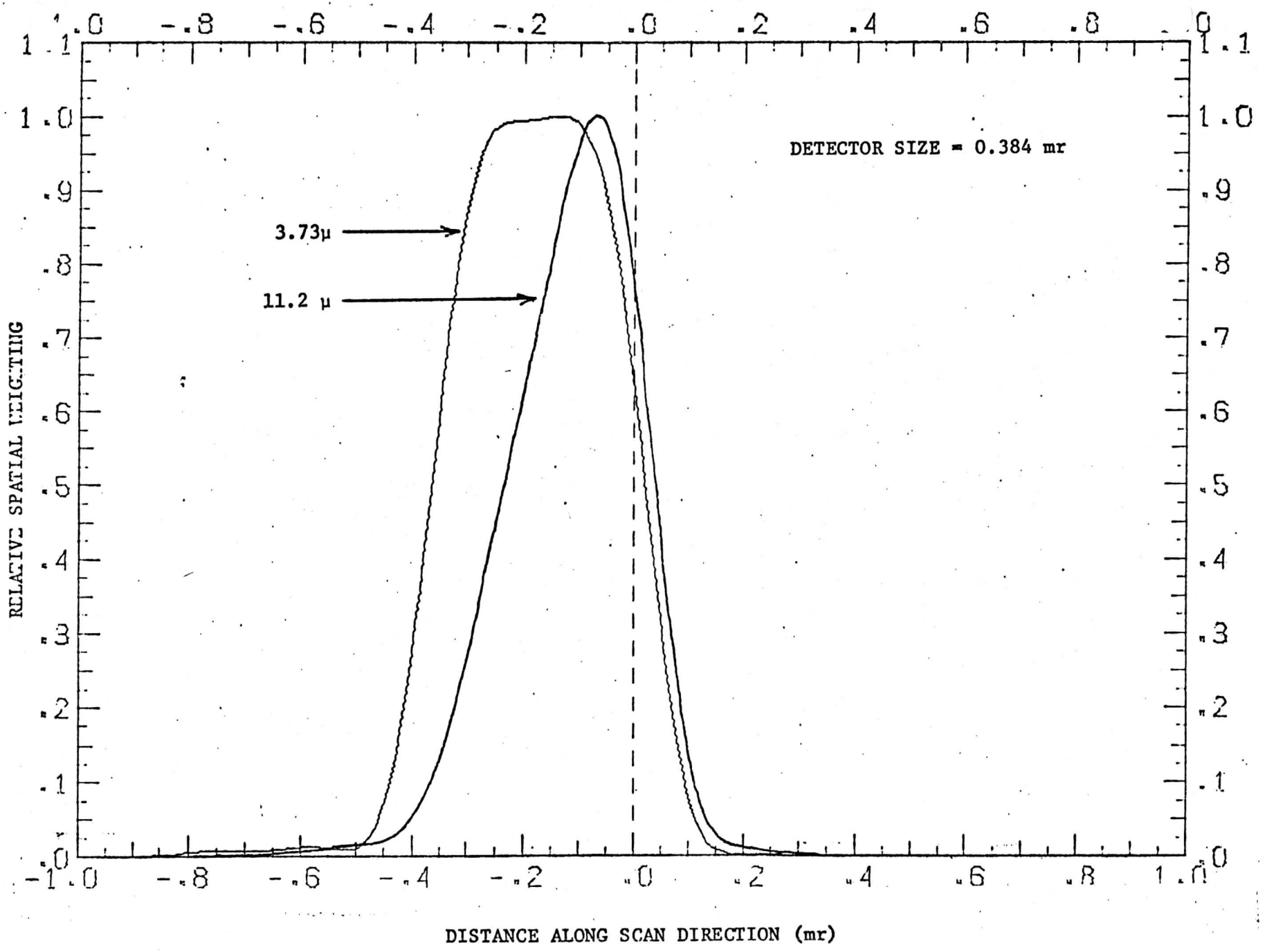

Figure 1.7. Relative spatial weighting of 11.2μ and 3.73μ bands along the E-W (scan) direction. The major difference in these functions is due to the nonuniform responsivity of HgCdTe detectors.

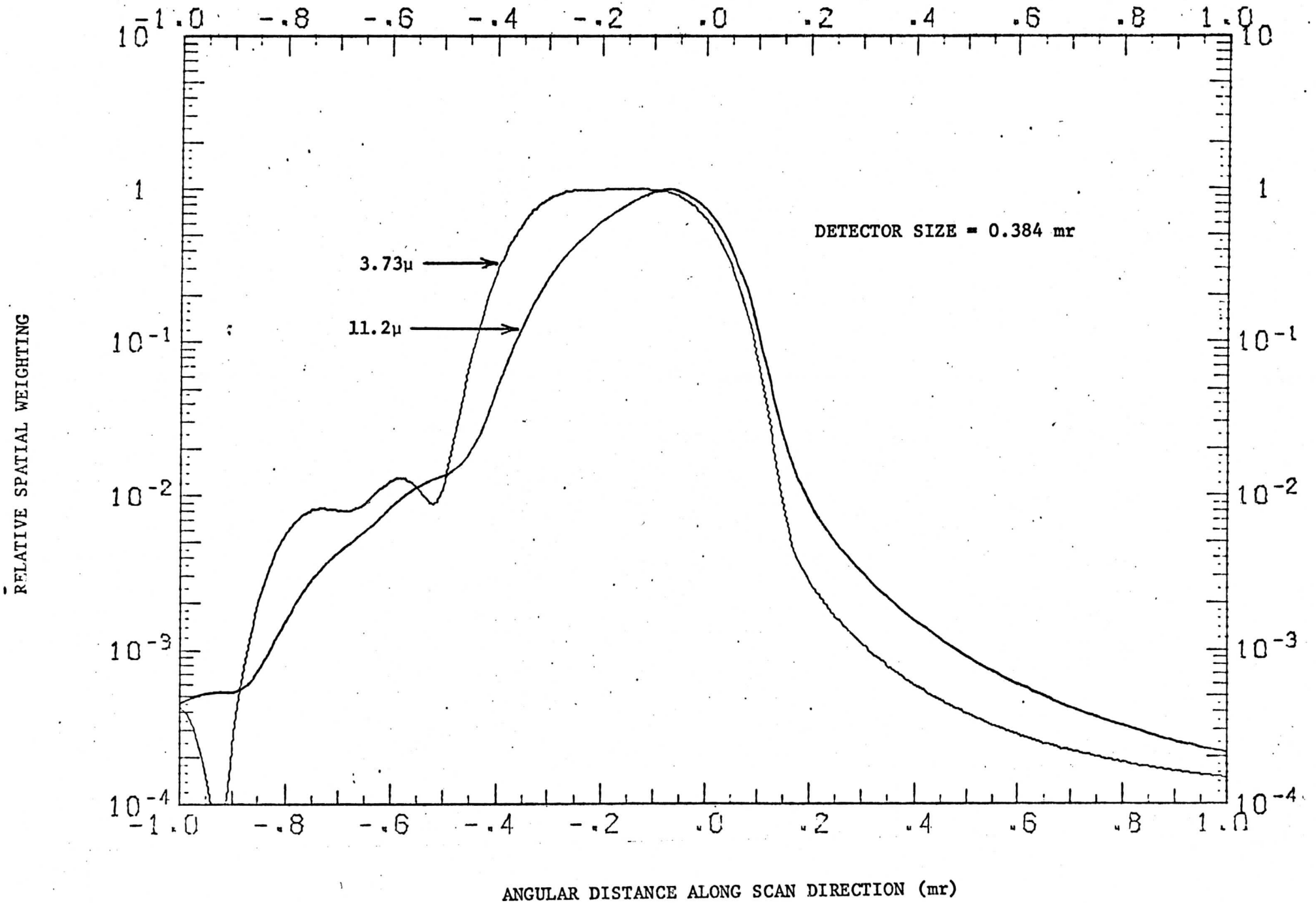

Figure 1.8. Relative Spatial Weighting of 3.73μ and 11.2μ bands. This is a semi-log version of Figure 1.3. Differences in the tails are a result of a different diffraction patterns